Optogenetic acidification of synaptic vesicles and lysosomes

Benjamin R Rost[1,2,8], Franziska Schneider[3,7,8], M Katharina Grauel[1], Christian Wozny[1,4], Claudia G Bentz[1], Anja Blessing[5,6], Tanja Rosenmund[1], Thomas J Jentsch[5,6], Dietmar Schmitz[1,2], Peter Hegemann[3] & Christian Rosenmund[1]

© 2015 Nature America, Inc. All rights reserved.

Acidification is required for the function of many intracellular organelles, but methods to acutely manipulate their intraluminal pH have not been available. Here we present a targeting strategy to selectively express the light-driven proton pump Arch3 on synaptic vesicles. Our new tool, pHoenix, can functionally replace endogenous proton pumps, enabling optogenetic control of vesicular acidification and neurotransmitter accumulation. Under physiological conditions, glutamatergic vesicles are nearly full, as additional vesicle acidification with pHoenix only slightly increased the quantal size. By contrast, we found that incompletely filled vesicles exhibited a lower release probability than full vesicles, suggesting preferential exocytosis of vesicles with high transmitter content. Our subcellular targeting approach can be transferred to other organelles, as demonstrated for a pHoenix variant that allows light-activated acidification of lysosomes.

The release of neurotransmitters from synaptic vesicles is a key element of chemical synaptic transmission. Synaptic vesicle recycling after exo- and endocytosis requires neurotransmitter uptake by specialized vesicular transporter proteins[1]. The electrochemical driving force for neurotransmitter accumulation is generated by vacuolar-type H^+-ATPases (V-ATPases) that actively transport cytosolic protons into the synaptic vesicle lumen, thereby acidifying the vesicles and generating an inside-positive membrane potential[2]. V-ATPases also acidify other subcellular compartments of the secretory and endocytic pathways, such as endosomes, Golgi-derived vesicles and lysosomes, but to a different extent, with lysosomes being the most acidic compartments in a cell (pH < 5) (ref. 3). The tightly regulated acidification of these organelles is a prerequisite for a plethora of different processes, including processing, storage and degradation of proteins, lipids and polysaccharides[3,4]. However, elucidating the physiological roles of V-ATPases has remained challenging because we lack tools that allow rapid and compartment-specific control of proton accumulation.

The recent advance of optogenetic methods allows precise manipulation of many cellular activities with light. In neuroscience, microbial rhodopsins such as channelrhodopsins and light-activated ion pumps are applied to modulate the neuronal membrane potential, thereby tuning excitability[5–7]. Cell-type-specific expression of such actuators is commonly achieved by combining sophisticated expression systems with specific promoters[8], but only few publications report cell-compartment-specific expression of optogenetic actuators, including expression in the postsynaptic density[9], in dendrites[10] and in axon initial segments[11,12]. While these tools allow manipulation of the local plasma membrane potential, optogenetic tools to control the ion and voltage gradients across intracellular membranes in neurons have not yet been developed. Here we report a strategy to express the light-activated proton pump Archaerhodopsin-3 (Arch3)[7,13] from *Halorubrum sodomense* on synaptic vesicles, together with the pH-sensitive GFP variant pHluorin as sensor for vesicular pH[14]. The fusion protein, named pHoenix, enables controlling and monitoring acidification of synaptic vesicles by yellow and blue light, respectively. We applied pHoenix to manipulate the neurotransmitter content of synaptic vesicles and to investigate the interplay of vesicle content and exocytosis. First, we found that additional optogenetic acidification slightly increased EPSC amplitudes, as well as quantal size. Second, we assessed whether insufficient filling of glutamatergic vesicles affects release probability. After pharmacological depletion of the synaptic vesicle content, we subsequently used pHoenix for optically controlled reacidification and restoration of transmitter uptake. We found that insufficiently filled vesicles fused with a lower probability. Drawing on the modular design of pHoenix, we also created a variant targeting lysosomes, enabling external control of lysosomal acidification.

RESULTS

Targeting Arch3 to synaptic vesicles

To functionally express a light-activated proton pump in the synaptic vesicle membrane, we incorporated Arch3 between helix three and four of the vesicular protein synaptophysin, together with the fluorescent proteins mKate2 on the cytosolic and pHluorin on the luminal side to indicate protein expression and localization, as well as luminal acidification. As the C terminus of Arch3 is located on the cytosolic

[1]Neuroscience Research Center, Charité – Universitätsmedizin Berlin, Berlin, Germany. [2]German Center for Neurodegenerative Diseases (DZNE), Berlin, Germany. [3]Institute of Biology, Experimental Biophysics, Humboldt-Universität zu Berlin, Berlin, Germany. [4]Institute of Pharmacy and Biomedical Sciences, University of Strathclyde, Glasgow, UK. [5]Max-Delbrück-Centrum für Molekulare Medizin (MDC), Berlin, Germany. [6]Leibniz-Institut für Molekulare Pharmakologie (FMP), Berlin, Germany. [7]Present address: National Heart and Lung Institute, Imperial College London, London, UK. [8]These authors contributed equally to this work. Correspondence should be addressed to B.R.R. (benjamin.rost@dzne.de).

Received 19 August; accepted 8 October; published online 9 November 2015; doi:10.1038/nn.4161

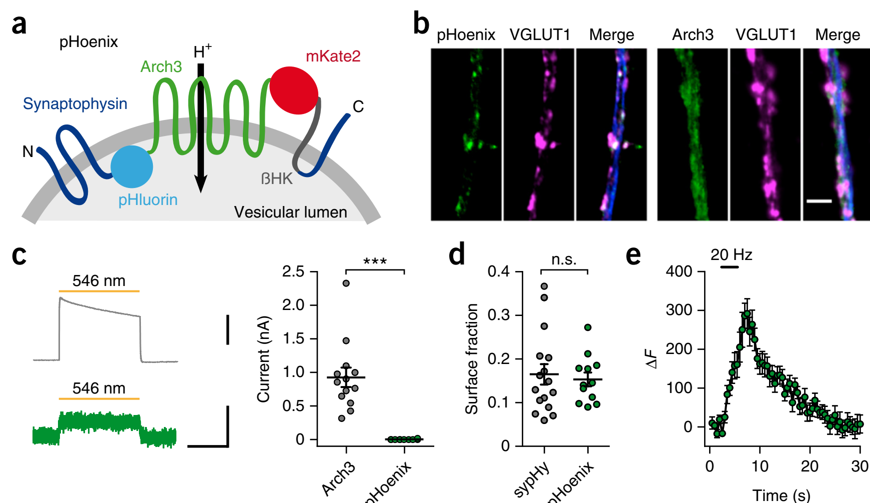

Figure 1 Design and localization of the light-driven vesicular proton pump pHoenix. (**a**) Membrane topology of the pHoenix construct. βHK: H^+/K^+ ATPase β-subunit. (**b**) Confocal images displaying a dendritic segment of a neuron expressing pHoenix or Arch3-eGFP (green), counterstained for the presynaptic marker VGLUT1 (magenta) and the dendritic marker MAP2 (blue). Scale bar, 3 µm. (**c**) Membrane currents evoked by brief light applications in Arch3- (upper trace; scale bar, 500 pA) or pHoenix-expressing neurons (lower trace; scale bars, 500 ms, 50 pA). Arch3-positive cells showed currents of 0.9 ± 0.1 nA (n = 13 cells, N = 2 cultures), while in pHoenix-positive cells light triggered only small currents (3.6 ± 2.1 pA, n = 8 cells, N = 2 cultures; ***P = 0.0002, Mann-Whitney U test, U = 0). (**d**) Surface fractions of sypHy and pHoenix at synaptic terminals were 0.17 ± 0.02 for sypHy (n = 16 cells) compared to 0.15 ± 0.02 for pHoenix (n = 12 cells, N = 3 cultures; P = 0.7, unpaired two-tailed t-test, t_{26} = 0.378). (**e**) Exocytosis triggered by 60 action potentials at 20 Hz increased pHluorin signals as a result of membrane fusion of pHoenix-containing synaptic vesicles (n = 11 cells, N = 4 cultures). n.s., not significant.

side[13] while the fourth synaptophysin helix originates in the vesicle lumen, we added the transmembrane helix of the rat gastric H^+/K^+ ATPase β-subunit (βHK) to maintain the transmembrane topology[15] (**Fig. 1a** and **Supplementary Fig. 1a**,**b**).

We expressed the resulting fusion protein, pHoenix, in mouse hippocampal neurons using lentivirus. After 2 weeks in culture, pHoenix was enriched at presynaptic terminals and colocalized with the vesicular glutamate transporter 1 (VGLUT1), which was not the case for untargeted Arch3-eGFP (**Fig. 1b**). During whole-cell patch-clamp recordings, 1-s light pulses evoked 250 times smaller somatic outward currents in pHoenix-expressing neurons than in neurons expressing Arch3-eGFP (**Fig. 1c**), indicating that pHoenix is mostly retained intracellularly. Indeed, optical quantification of surface-resident pHluorin molecules (**Supplementary Fig. 1c**,**d**) revealed that only 15% of the pHoenix proteins resided in the plasma membrane (**Fig. 1d**), similarly to synaptophysin-pHluorin (sypHy), a well-established indicator of vesicular pH and synaptic transmission[14]. Furthermore, bursts of 60 action potentials at 20 Hz triggered an increase of pHluorin fluorescence due to exocytosis of synaptic vesicles in pHoenix-expressing neurons (**Fig. 1e**), demonstrating proper integration of the construct into synaptic vesicles. Notably, expression of pHoenix did not interfere with basic neuronal release parameters (**Supplementary Fig. 2**).

Light-driven acidification of synaptic vesicles by pHoenix

V-ATPases acidify newly formed synaptic vesicles after their endocytosis from the presynaptic plasma membrane, providing the proton-motive force that drives the neurotransmitter uptake by specialized antiporters such as the vesicular glutamate transporters VGLUT1–3 (ref. 16). To test whether pHoenix could functionally substitute for the activity of the endogenous proton pumps, we blocked vesicular acidification and transmitter uptake by incubating cultured hippocampal neurons grown on microislands with the V-ATPase inhibitor bafilomycin A1 (Baf). We then monitored pHluorin signals in glutamatergic neurons to follow vesicle acidification and, in parallel, recorded excitatory postsynaptic currents (EPSCs), which indicated the degree of vesicular transmitter filling. Preincubation with 1 µM Baf for 2–5 h depleted the proton gradient over vesicular membranes and resulted in strong pHluorin fluorescence at synaptic terminals (**Fig. 2a**), with no or very small EPSCs evoked by action potentials (**Fig. 2b**). pHoenix activation with 580-nm light for 2 min resulted in a biphasic fluorescence decrease, with an immediate drop to 70% in the first 5 s, reflecting fast vesicle acidification, followed by a slower decay to 60% (**Fig. 2a**,**c**). Simultaneously recorded EPSCs recovered with a time constant τ = 58 s (**Fig. 2b**,**c**). Control experiments in neurons expressing sypHy showed that bleaching of pHluorin-molecules could not account for the rapid decrease of

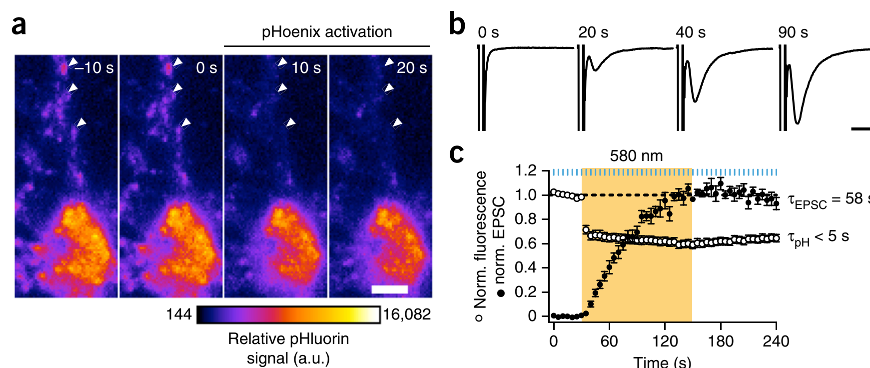

Figure 2 pHoenix can substitute for V-ATPase function. (**a**) pHluorin signals of a pHoenix-expressing, Baf-treated neuron acquired before (time point –10 and 0 s) and during (10 and 20 s) pHoenix activation. Arrowheads indicate synaptic contacts. Scale bar, 10 µm. (**b**) EPSCs recorded from a Baf-treated neuron at indicated time points during pHoenix activation. Scale bars, 5 ms and 1 nA. (**c**) Time plot of normalized pHluorin signals and normalized EPSCs recorded in parallel from Baf-treated, pHoenix-expressing cells (n = 15 cells, N = 2 cultures). Fluorescence of pHluorin molecules was imaged at 0.2 Hz using 100-ms flashes of a 490-nm LED (dotted blue line) just before action potentials were triggered. Vesicle acidification by pHoenix and transmitter uptake were induced by interlaced illumination with yellow light. Norm., normalized; a.u., arbitrary units.

© 2015 Nature America, Inc. All rights reserved.

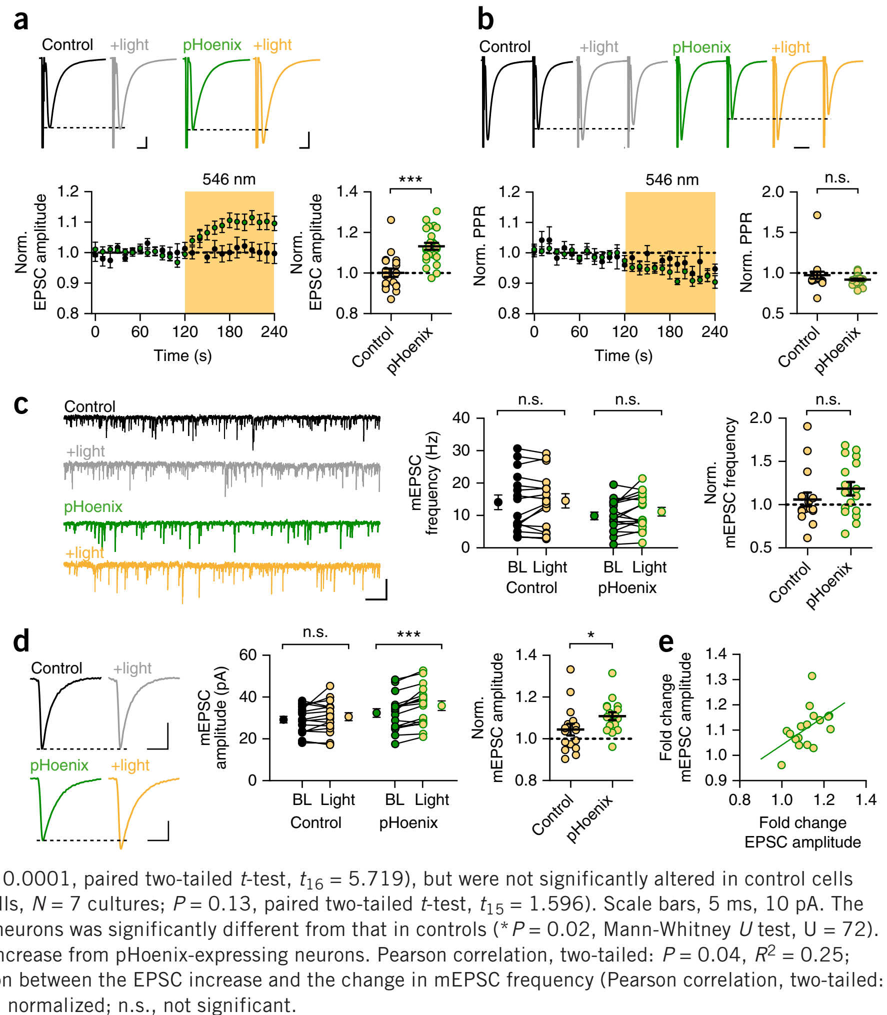

Figure 3 Activation of pHoenix in untreated neurons increases the quantal size. (**a**) Averages of four EPSCs recorded before and at the end of the 2-min illumination period from an uninfected control and a pHoenix-expressing neuron. Scale bars, 5 ms and 2 nA. Illumination had no effect on EPSCs evoked at 0.1 Hz in control neurons (0.1 ± 2%, $n = 19$ cells, $N = 7$ cultures), but increased EPSCs in pHoenix-expressing neurons by 13 ± 2% ($n = 24$ cells, $N = 7$ cultures; $***P < 0.0001$, Mann-Whitney U test; $U = 55$). (**b**) Example traces of paired EPSCs evoked at 40-ms inter-stimulus interval. Amplitudes normalized to the first EPSC. Scale bar, 10 ms. Paired-pulse ratio changes were not different between the control and pHoenix group ($P = 0.1$, two-tailed Mann-Whitney U test, $U = 159$). (**c**) Spontaneous quantal release events were analyzed from 1-min periods preceding light and the second minute of illumination. Light did not alter the frequency of mEPSCs (control cells: baseline (BL): 14.1 ± 2.3 Hz, light: 14.5 ± 2.2 Hz; $n = 16$ cells, $N = 7$ cultures; $P = 0.5$, paired two-tailed t-test, $t_{15} = 0.701$; pHoenix cells: BL = 9.9 ± 1.2 Hz, light: 11.2 ± 1.4 Hz; $n = 17$ cells, $N = 7$ cultures; $P = 0.1$, paired two-tailed t-test, $t_{16} = 1.809$). Scale bar, 200 ms and 50 pA. The mEPSC frequency change in pHoenix expressing cells was not significantly different from that in control neurons ($P = 0.2$, Mann-Whitney U test, $U = 102$). (**d**) mEPSC amplitudes increased significantly in pHoenix expressing neurons (BL: 32.4 ± 2.1 pA, light: 35.9 ± 2.3 pA, $n = 17$ cells, $N = 7$ cultures; $***P < 0.0001$, paired two-tailed t-test, $t_{16} = 5.719$), but were not significantly altered in control cells (BL: 29.2 ± 1.6 pA, light: 30.6 ± 1.9 pA; $n = 16$ cells, $N = 7$ cultures; $P = 0.13$, paired two-tailed t-test, $t_{15} = 1.596$). Scale bars, 5 ms, 10 pA. The increase of mEPSC amplitudes in pHoenix-positive neurons was significantly different from that in controls ($*P = 0.02$, Mann-Whitney U test, U = 72). (**e**) Correlation of the EPSC and mEPSC amplitude increase from pHoenix-expressing neurons. Pearson correlation, two-tailed: $P = 0.04$, $R^2 = 0.25$; $n = 17$ cells, $N = 7$ cultures. There was no correlation between the EPSC increase and the change in mEPSC frequency (Pearson correlation, two-tailed: $P = 0.25$, $R^2 = 0.09$; correlation not shown). Norm., normalized; n.s., not significant.

© 2015 Nature America, Inc. All rights reserved.

npg

fluorescence (**Supplementary Fig. 3**). Thus, pHoenix activity is sufficient to rapidly acidify synaptic vesicles, allowing the control of vesicular transmitter uptake with light.

We further tested the applicability of pHoenix in organotypic brain slices. Adeno-associated virus encoding pHoenix was injected into area CA3 after 3 to 5 d *in vitro* (**Supplementary Fig. 4a**). At >14 d after infection, we incubated slices with 1 μM Baf overnight, which caused strong pHluorin signals (**Supplementary Fig. 4b**) and effectively abolished EPSCs. pHoenix activation for 2 min recovered synaptic transmission at associational-commissural fiber synapses (**Supplementary Fig. 4c**,**d**), illustrating that the use of pHoenix can also be extended to brain slice preparations and possibly *in vivo* applications.

Refilling of synaptic vesicles by pHoenix should create a finite pool of vesicles that could be subsequently depleted by action potential–triggered exocytosis. Indeed, following 2 min of illumination and pHoenix-mediated recovery of transmission, repetitive stimulation with trains of action potentials (600 action potentials over 300 s), but not sparse stimulation (30 action potentials in 300 s), rapidly reduced EPSC amplitudes in autaptic cultures of glutamatergic neurons (**Supplementary Fig. 5**). Accordingly, pHluorin signals strongly increased under the train stimulation because of the exhaustive exocytosis and failure of reacidification. A second illumination period caused requenching of pHluorin signals, while synaptic transmission recovered, illustrating that optogenetic vesicle acidification and transmitter uptake is fully reversible by action potential–driven exocytosis.

The observed rescue of transmission in Baf-treated neurons was pHoenix-specific: while light-induced EPSC recovery in pHoenix-expressing cells yielded EPSCs of 3.1 ± 0.6 nA, illumination failed to rescue EPSCs in control cells expressing Arch3-eGFP (**Supplementary Fig. 6a**). Rescued EPSCs of Baf-treated neurons reached amplitudes comparable to those of EPSCs of untreated cells from the same culture (**Supplementary Fig. 6b**). Furthermore, the frequency and amplitude of spontaneous miniature EPSCs (mEPSCs), which reflect the stochastic fusion of single vesicles, did not differ between the two groups (**Supplementary Fig. 6c**). Thus, the light-driven pHoenix activity can achieve vesicular transmitter filling comparable to that of endogenous V-ATPases.

Superfilling of synaptic vesicles by pHoenix activity

EPSCs of untreated neurons expressing pHoenix slightly increased during illumination (**Supplementary Fig. 6b**). We characterized this effect in detail by comparing pHoenix-expressing neurons with control neurons (uninfected or sypHy-infected). Activation of pHoenix increased EPSC amplitudes by 13 ± 2%, an effect not seen in controls (**Fig. 3a**). We directly assessed the release probability in these cells by using a 40-ms paired-pulse stimulation protocol, wherein a low ratio of the second to first EPSC amplitude indicates a high release probability[17]. The light-induced change in the paired-pulse ratio (PPR) was not significantly different between the two groups (**Fig. 3b**), and thus the increase of EPSC amplitudes was probably not due to a

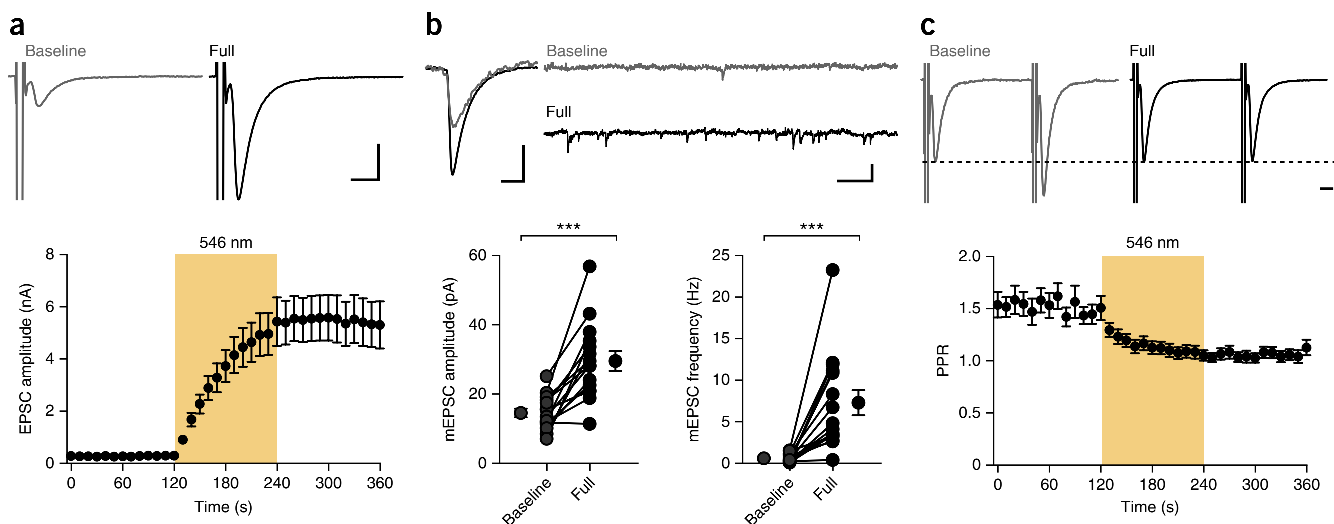

Figure 4 Neurons with residual glutamate release after Baf-treatment have smaller mEPSCs and a high paired-pulse ratio. (**a**) Residual EPSC of a neuron incubated for 165 min in Baf (baseline, gray trace), which increased to 400% after pHoenix activation (full, black trace). Scale bars, 5 ms, 0.5 nA. EPSC recovery shown for 20 cells with residual release (0.3 ± 0.1 nA before, 5.5 ± 0.9 nA after illumination, τ = 66 s; *N* = 7 cultures). (**b**) Average mEPSCs and example trace of mEPSCs recorded from a neuron before (gray) and after (black) activation of pHoenix. Scale bars, left: 5 ms and 10 pA; right: 100 ms and 50 pA. mEPSC amplitudes increased from 17 ± 2 to 29 ± 3 pA, and mEPSC frequency increased from 0.7 ± 0.2 to 8.1 ± 1.7 Hz (*n* = 15 cells, *N* = 7 cultures; amplitudes: ***$P < 0.0001$, paired two-tailed *t*-test, $t_{14} = 5.847$; frequency: ***$P < 0.0001$, Wilcoxon signed-rank test, *W* = –120). (**c**) Paired EPSCs evoked at 40-ms intervals during baseline and after pHoenix activation. Amplitudes scaled to first EPSC. Scale bar, 5 ms. Time course shows the PPR change from the same cells as in **a**. PPR decreased from 1.5 ± 0.1 to 1.1 ± 0.1, with τ = 23 s.

higher release probability. Likewise, illumination did not have a differential effect on the mEPSC frequency (**Fig. 3c**). However, illumination caused a significant increase of mEPSCs amplitudes by 11 ± 2% (**Fig. 3d**) in pHoenix-expressing cells. Our experiments suggest that light-activated proton pumping by pHoenix provides an additional driving force for vesicular transmitter accumulation, reflected by larger postsynaptic responses (**Fig. 3e**), but the relatively small effect on both EPSC and mEPSC amplitudes implies that vesicles are nearly filled to maximal storage capacity under physiological conditions.

Partially filled vesicles have a lower release probability

Reliable synaptic transmission requires exocytosis of synaptic vesicles loaded with sufficient levels of neurotransmitter molecules. However, whether incomplete vesicular filling affects vesicle release probability is still under debate. In fact, some experiments have found the vesicular fill state to influence vesicle release probability[18,19], while others have found equally efficient release of empty vesicles[20,21]. The ability to control transmitter uptake into vesicles by light-driven proton pumping allowed us to directly assess the relation of vesicular transmitter content and vesicular release probability. We investigated transmitter release of autaptic neurons that still exhibited small, residual EPSCs after >2 h incubation in Baf and compared it to the restored release after pHoenix activation (**Fig. 4a**). pHoenix-driven transmitter uptake increased mEPSC amplitudes by 70%, while mEPSC frequency increased more than tenfold (**Fig. 4b**). The small initial mEPSC amplitudes imply that residual EPSCs rely on vesicles only partially filled with glutamate. Notably, the PPR decreased by 40% during the pHoenix-mediated EPSC recovery (**Fig. 4c**), indicating that vesicular release probability increases with vesicular filling. The incrementing release of glutamate could lead to a progressive desensitization of postsynaptic AMPA receptors, which might contribute to changes in the PPR[22]. However, in the presence of cyclothiazide, an antagonist of AMPA receptor desensitization, we observed a comparable decrease in PPR (**Supplementary Fig. 7**), ruling out the possibility that in our experimental conditions the increased vesicular content enhances receptor desensitization.

The high PPR of residual EPSCs might result from the release of a pool of 'release-reluctant' vesicles that were not discharged during the incubation with Baf because of an intrinsically low release probability. As pHoenix activity promotes gradual filling of synaptic vesicles, we were able to titrate the vesicular glutamate content more accurately using a two-step recovery protocol: in cells devoid of transmission after Baf treatment, we applied a 30-s nonsaturating light pulse that caused only partial recovery of the evoked response, followed by a dark phase of 60 s and a second saturating light pulse for 90 s (**Fig. 5a**). This protocol allowed us to compare an intermediate fill state with reduced postsynaptic responses to the condition with full vesicles after final EPSC recovery. In the intermediate fill state, EPSCs remained stable, at 37% of the final amplitude, while pHluorin signals increased slightly as a result of action potential–triggered exocytosis (**Supplementary Fig. 8**). This indicates that VGLUTs require constant proton pumping for transmitter uptake. Using two independent approaches, we verified that the nonsaturating light pulse created partially filled vesicles. First, analysis of spontaneous release revealed that mEPSC amplitudes were 25% smaller and occurred at a 42% lower frequency compared to the full recovery state (**Fig. 5b**). Second, we tested the effectiveness of the low-affinity, competitive AMPAR antagonist γ-D-glutamylglycine (γ-DGG) on attenuating EPSCs, which has been established as an indicator of the amount of vesicular glutamate released by exocytosis[23]: a strong reduction of EPSCs by γ-DGG reflects a low vesicular glutamate content, whereas the γ-DGG effect decreases with increasing amounts of glutamate released. We found that after the nonsaturating light interval, γ-DGG decreased EPSCs to 31%, while EPSCs were reduced to only 40% after the second, saturating light interval (**Fig. 5c**). Both observations support the idea that the reduced postsynaptic responses in the intermediate recovery are based on a partial vesicular fill state.

© 2015 Nature America, Inc. All rights reserved.
npg

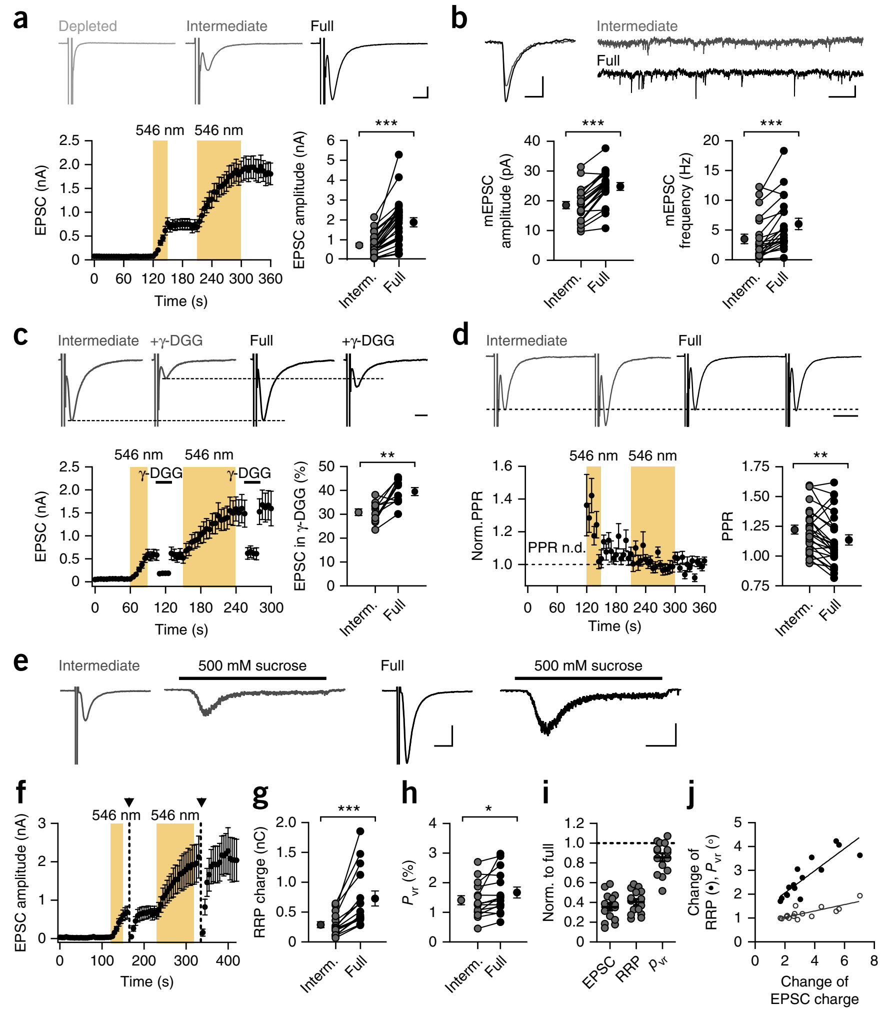

Figure 5 Partially filled vesicles have a lower release probability. (**a**) Interval activation of pHoenix allows titration of EPSCs from a depleted to an intermediate (interm.) and full recovery state. Scale bars, 5 ms, 200 pA. EPSCs recovered during the 30 s of pHoenix activation to 0.7 ± 0.1 nA, remained stable during the intermediate dark phase and further increased over the following 90 s of illumination to 1.9 ± 0.2 nA (n = 26 cells, N = 6 cultures, ***P < 0.0001, Wilcoxon signed-rank test, W = −351). (**b**) Averages of mEPSCs detected during intermediate (gray) and full recovery condition (black), with typical mEPSC recordings from the same cell. Scale bars, left: 5 ms, 10 pA; right: 200 ms, 25 pA. mEPSC amplitudes increased from 18.6 ± 1.2 to 24.9 ± 1.3 pA (n = 21 cells, N = 6 cultures; ***P < 0.0001, paired two-tailed t-test, t_{20} = 9.811), while the frequency increased from 3.5 ± 0.8 to 6.0 ± 1.0 Hz (***P = 0.0002, Wilcoxon signed-rank test, W = −217). (**c**) Attenuation of EPSCs by the application of γ-DGG. EPSCs scaled to EPSCs before drug application. Scale bar, 5 ms. γ-DGG application caused an instantaneous drop of EPSC amplitudes (n = 10 cells; N = 2 cultures). The EPSC reduction was stronger during the intermediate fill state than during the full recovery state (**P = 0.003, paired two-tailed t-test, t_9 = 4.155). (**d**) Average traces of paired EPSCs during intermediate and full recovery conditions, normalized to the first EPSC. Scale bar, 10 ms. PPR time course during the interval recovery protocol, normalized to the period after the second light interval. During the intermediate recovery state, average PPR was significantly higher than after full recovery (intermediate: 1.22 ± 0.04, full: 1.14 ± 0.04; n = 26 cells, N = 6 cultures; **P = 0.004, paired two-tailed t-test, t_{25} = 3.222). (**e**) Postsynaptic response elicited by application of 500 mM sucrose after intermediate and full recovery of transmission. Averages of EPSCs recorded after the first and the second light interval are shown for comparison. Scale bars, 10 ms, 1 nA for EPSCs; 1 s, 1 nA for sucrose responses. (**f**) Hypertonic sucrose solution was applied (arrows) after the first and second light intervals. EPSC amplitudes recovered after the depletion of the RRP (n = 15 cells, N = 4 cultures). (**g**) The RRP increased from 290 ± 50 pC to 730 ± 130 pC (***P = 0.0002, paired two-tailed t-test, t_{14} = 5.116). (**h**) The p_{vr} increased from 1.4 ± 0.2% to 1.7 ± 0.2% (*P = 0.02, paired two-tailed t-test, t_{14} = 2.665). (**i**) EPSC charge, RRP and p_{vr} during the intermediate state normalized to the full recovery state. (**j**) The increase of the EPSC from the intermediate to the full recovery state correlates with the increase of the RRP (Pearson correlation, P < 0.0001, R^2 = 0.75) and the p_{vr} (Spearman correlation, P = 0.003). Norm., normalized.

© 2015 Nature America, Inc. All rights reserved.

npg

How does partial transmitter filling affect the release probability? Paired-pulse measurements showed a 10% higher PPR in the intermediate recovery state compared to the full state (**Fig. 5d**), indicating a lower release probability of partially filled vesicles. We also assessed the readily releasable pool (RRP) of synaptic vesicles by brief applications of hypertonic sucrose solutions during the intermediate and the final recovery state (**Fig. 5e**,**f**), which allowed us to directly calculate the vesicular release probability (p_{vr})[24]. During the intermediate recovery state, the RRP was 60% smaller than in the final recovery state (**Fig. 5g**,**i**). The p_{vr} of partially filled vesicles was 14% lower than that of vesicles after complete filling (**Fig. 5h**,**i**), and the vesicular fill state correlated with the pool size and p_{vr} (**Fig. 5j**). Thus, insufficient vesicular filling reduces the vesicular release probability.

Light-driven acidification of lysosomes

The modular pHoenix design provides a blueprint for specific intracellular trafficking of both Arch3 and fluorescent indicators. Consequently, we modified pHoenix to target lysosomes by insertion of the pHluorin-Arch3-mKate2-βHK construct between helix 1 and 2 of the tetraspanin CD63, a lysosomal marker protein[25] (**Fig. 6a**). The resulting protein, lyso-pHoenix, showed strong colabeling with the lysosome-associated membrane protein 2 (LAMP2), but not with markers for the Golgi apparatus, endoplasmic reticulum, endosome or mitochondria, demonstrating specific expression on lysosomal membranes (**Fig. 6b**,**c** and **Supplementary Fig. 9**). In Baf-treated HEK 293 cells, activation of lyso-pHoenix by 580-nm light caused a rapid decrease of pHluorin signals, indicating a drop in pH, which was not seen in control cells expressing CD63-pHluorin. Remarkably, lysosomal acidification required constant proton pumping, as pHluorin signals quickly recovered after termination of lyso-pHoenix activation, suggesting a strong proton leak in lysosomes (**Fig. 6d**).

DISCUSSION

Light-driven proton pumps are powerful tools for silencing neuronal activity, as they hyperpolarize the plasma membrane by exporting protons from the cytosol to the extracellular side of the membrane[26]. However, only few studies have exploited their potential to alter the pH of intracellular organelles. In yeast, the light-driven proton pump

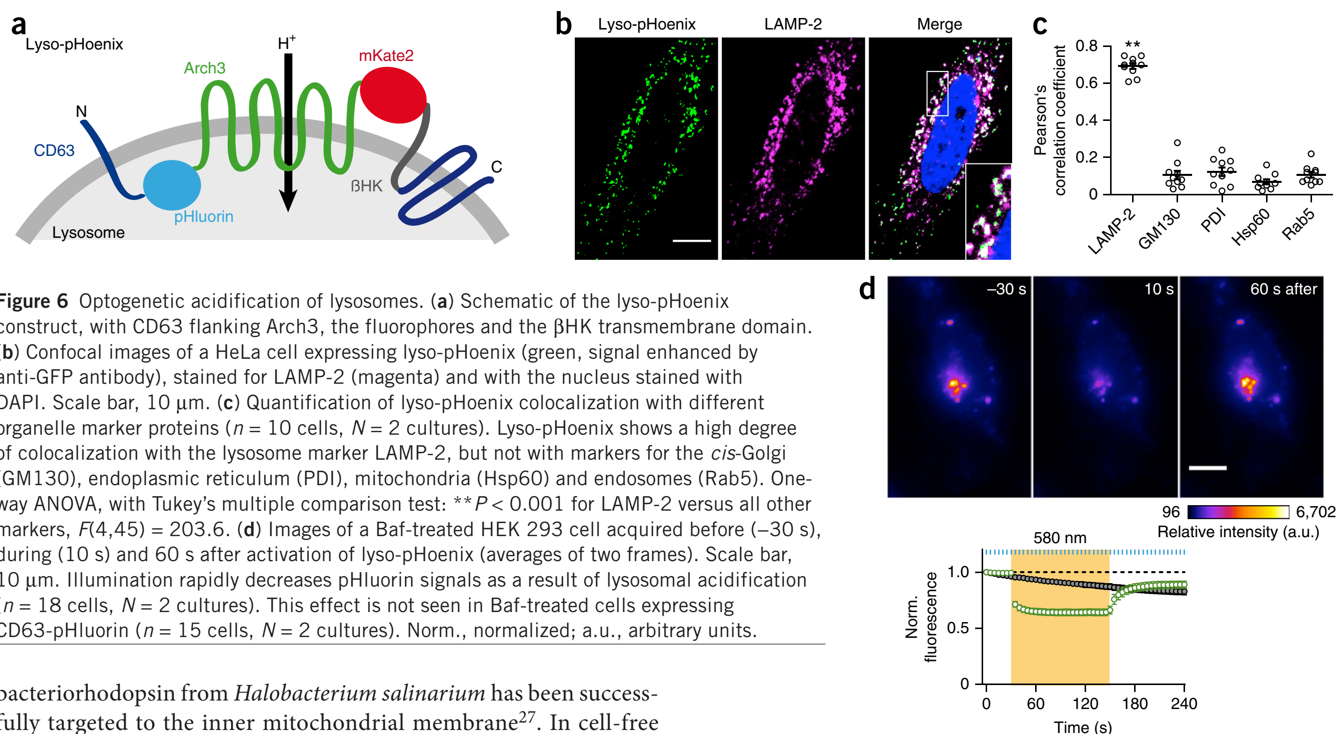

Figure 6 Optogenetic acidification of lysosomes. (**a**) Schematic of the lyso-pHoenix construct, with CD63 flanking Arch3, the fluorophores and the βHK transmembrane domain. (**b**) Confocal images of a HeLa cell expressing lyso-pHoenix (green, signal enhanced by anti-GFP antibody), stained for LAMP-2 (magenta) and with the nucleus stained with DAPI. Scale bar, 10 μm. (**c**) Quantification of lyso-pHoenix colocalization with different organelle marker proteins (n = 10 cells, N = 2 cultures). Lyso-pHoenix shows a high degree of colocalization with the lysosome marker LAMP-2, but not with markers for the *cis*-Golgi (GM130), endoplasmic reticulum (PDI), mitochondria (Hsp60) and endosomes (Rab5). One-way ANOVA, with Tukey's multiple comparison test: $**P < 0.001$ for LAMP-2 versus all other markers, $F(4,45) = 203.6$. (**d**) Images of a Baf-treated HEK 293 cell acquired before (–30 s), during (10 s) and 60 s after activation of lyso-pHoenix (averages of two frames). Scale bar, 10 μm. Illumination rapidly decreases pHluorin signals as a result of lysosomal acidification (n = 18 cells, N = 2 cultures). This effect is not seen in Baf-treated cells expressing CD63-pHluorin (n = 15 cells, N = 2 cultures). Norm., normalized; a.u., arbitrary units.

bacteriorhodopsin from *Halobacterium salinarium* has been successfully targeted to the inner mitochondrial membrane[27]. In cell-free assays, bacteriorhodopsin from *Halobacterium halobium* has been used to acidify proteoliposomes in order to study the proton dependence of VGLUT-driven glutamate uptake[28], but similar experiments have not yet been feasible in living neurons. Our new tool, pHoenix, now allows precise temporal control of the acidification process in synaptic vesicles and will enable studies on synaptic vesicle biogenesis and neurotransmitter uptake in living neurons.

Two parameters affect the vesicular transmitter filling: the proton gradient and the number and activity of vesicular transmitter transporters. Experimentally, the vesicular transmitter content can be manipulated in two ways: either by altering the number of active vesicular transmitter transporters[19,29–31] or by altering the proton electrochemical gradient[20,21]. To our knowledge, pHoenix is the first tool enabling acute increase of the vesicular proton gradient. In cells with intact V-ATPase function, additional optogenetic acidification increased both EPSC and mEPSC amplitudes by more than 10%. The ability of pHoenix to increase the vesicular glutamate filling beyond the filling capacity provided by V-ATPases demonstrates that Arch3 generates a proton motive force that exceeds the driving force provided by endogenous V-ATPases, indicating that the proton transport properties of V-ATPases limit the amount of glutamate uptake. The EPSC amplitude increase by pHoenix activation in untreated neurons also implies that activation of surface-resident pHoenix does not cause appreciable synaptic cleft acidification, which would impair synaptic transmission by inhibiting presynaptic calcium influx through voltage-gated calcium channels[32].

In Baf-treated neurons, refilling of vesicles by interval illumination revealed that glutamate uptake requires constant proton pumping (**Supplementary Fig. 8**). While pH remained low, glutamate uptake stopped immediately after light off and cessation of pHoenix activity. This is strong evidence for the idea that membrane voltage and not the pH gradient is the driving force for VGLUT-mediated transmitter uptake[2]. The absence of proton leakage and stable synaptic transmission during low-frequency stimulation indicates that both the low luminal pH and the transmitter content of glutamatergic synaptic vesicles are preserved even in the absence of V-ATPase function, arguing against a steady-state model of transmitter uptake and leak in synaptic vesicles[33]. This is not the case for lysosomes, where the pH increased again within seconds after terminating the lyso-pHoenix-mediated acidification, demonstrating constant lysosomal proton leakage.

Our experiments further revealed that partially filled neurotransmitter vesicles can be released, proving that exocytosis is not guarded by a rigid fill-state control mechanism. However, incompletely filled vesicles did have a lower release probability. The underlying mechanism for this observation is not clear, but it seems likely that proton pumping and transmitter accumulation increase intravesicular osmolarity, which leads to a higher vesicle membrane tension and increases fusion probability with the plasma membrane. Electron microscopy studies reveal that synaptic vesicles of VGLUT1-deficient neurons are deformed in comparison to vesicles from wild-type neurons, suggesting that failure of transmitter uptake (but not failure of acidification) renders them more labile[19,34]. Moreover, filled vesicles have a larger diameter than empty vesicles[35,36]. Notably, the PPR changed faster than EPSCs increased, both at high (**Fig. 4**) and low illumination intensity (**Supplementary Fig. 7**), indicating that the threshold for a high p_{vr} defined by intravesicular osmolarity and membrane tension is reached before the maximal vesicular transmitter storage capacity. In line with this, we observed no further increase of the release probability when we used pHoenix in untreated cells to further increase vesicular filling (**Fig. 3**). The preferential release of completely filled vesicles could be of relevance for synaptic information processing: during sustained neuronal firing and high turnover of vesicles, this mechanism might assure efficient postsynaptic receptor activation and reliable synaptic transmission.

As pHoenix can functionally replace V-ATPases, it can be applied to rescue the cellular degeneration observed in V-ATPase knockout models in yeast[37], *Drosophila*[38] and mice[39]. Recent studies have suggested that V-ATPases have acidification-independent functions as vesicular pH sensors[40] and interaction partners of SNARE proteins[41], and may participate directly in synaptic vesicle fusion[42].

© 2015 Nature America, Inc. All rights reserved.

npg

In combination with pump activity–deficient V-ATPase mutants[43], pHoenix will facilitate structure–function analyses of V-ATPases and help to elucidate their noncanonical functions.

Optogenetic organelle acidification allows the investigation of quantitative aspects of proton-dependent transport and to study the properties of organelles as a function of their intraluminal pH. To further pursue this goal, we tried to develop a variant with opposing function to pHoenix by replacing Arch3 by a channelrhodopsin with high proton conductance to deplete proton gradients using light. Unfortunately, all tested channelrhodopsin-derived pHoenix variants were ineffective (data not shown), probably because the multimerization properties of channelrhodopsins and microbial pumps differ[44–46]. Thus, a pHoenix-based actuator that allows manipulation of circuit activity will require further development of the construct.

Whereas the transfer of the pHoenix concept to other microbial-type rhodopsins has so far proven unsuccessful, we were able to target a pHoenix variant to a different subcellular compartment by replacing the synaptophysin parts in pHoenix with the lysosomal CD63 protein. The resulting lyso-pHoenix can be applied to specifically investigate the pH dependency of the catabolic processes confined to lysosomes; for example, the acid-dependent activity of lysosomal proteases[47]. Notably, alterations in organelle pH-homeostasis due to defects in proton translocation or counterion conductances are associated with many different pathophysiological conditions[48], ranging from cancer[49] to neurodegeneration[50]. The pHoenix constructs presented here may provide a new approach for directly assessing the role of acidification in these disorders.

METHODS

Methods and any associated references are available in the online version of the paper.

Accession codes. GenBank: pHoenix, KT880224; lyso-pHoenix, KT880225; lyso-pHluorin, KT880226.

Note: Any Supplementary Information and Source Data files are available in the online version of the paper.

ACKNOWLEDGMENTS

We thank K. Rösler, B. Brokowski, A. Felies, B. Söhl-Kielczynski, C. Schweynoch, J. Pustogowa and A. Schönherr for excellent technical support, the viral core facility of the Charité for virus production, and M. Camacho-Perez, S. Watanabe and A. Liebkowsky for critical comments on the manuscript. The work was supported by the German Research Council grants Cluster of Excellence Neurocure (EXC 257), Collaborative Research Center SFB958 (D.S., C.R.), Collaborative Research Center SFB1078 (F.S., P.H.), and the Integrative Research Institute for the Life Sciences (D.S., P.H., C.R.), a European Research Council grant (249939 SYNVGLUT; C.R.), a Grass Foundation Fellowship (B.R.R.) and the Louis-Jeantet Foundation (F.S., P.H.).

AUTHOR CONTRIBUTIONS

B.R.R. and F.S. developed the concepts for the pHoenix constructs. F.S. performed the molecular biology. B.R.R., F.S., M.K.G., C.W., C.G.B., A.B. and T.R. performed the experiments and analyzed the data. All authors designed the experiments and discussed the results. B.R.R. and F.S. prepared the manuscript, and all authors contributed to editing the paper.

COMPETING FINANCIAL INTERESTS

The authors declare no competing financial interests.

Reprints and permissions information is available online at http://www.nature.com/reprints/index.html.

1. Blakely, R.D. & Edwards, R.H. Vesicular and plasma membrane transporters for neurotransmitters. *Cold Spring Harb. Perspect. Biol.* **4**, 1–24 (2012).
2. Omote, H., Miyaji, T., Juge, N. & Moriyama, Y. Vesicular neurotransmitter transporter: bioenergetics and regulation of glutamate transport. *Biochemistry* **50**, 5558–5565 (2011).
3. Mindell, J.A. Lysosomal acidification mechanisms. *Annu. Rev. Physiol.* **74**, 69–86 (2012).
4. Forgac, M. Vacuolar ATPases: rotary proton pumps in physiology and pathophysiology. *Nat. Rev. Mol. Cell Biol.* **8**, 917–929 (2007).
5. Boyden, E.S., Zhang, F., Bamberg, E., Nagel, G. & Deisseroth, K. Millisecond-timescale, genetically targeted optical control of neural activity. *Nat. Neurosci.* **8**, 1263–1268 (2005).
6. Han, X. & Boyden, E.S. Multiple-color optical activation, silencing, and desynchronization of neural activity, with single-spike temporal resolution. *PLoS ONE* **2**, e299 (2007).
7. Chow, B.Y. *et al.* High-performance genetically targetable optical neural silencing by light-driven proton pumps. *Nature* **463**, 98–102 (2010).
8. Yizhar, O., Fenno, L.E., Davidson, T.J., Mogri, M. & Deisseroth, K. Optogenetics in neural systems. *Neuron* **71**, 9–34 (2011).
9. Gradinaru, V. *et al.* Targeting and readout strategies for fast optical neural control *in vitro* and in vivo. *J. Neurosci.* **27**, 14231–14238 (2007).
10. Greenberg, K.P., Pham, A. & Werblin, F.S. Differential targeting of optical neuromodulators to ganglion cell soma and dendrites allows dynamic control of center-surround antagonism. *Neuron* **69**, 713–720 (2011).
11. Grubb, M.S. & Burrone, J. Channelrhodopsin-2 localised to the axon initial segment. *PLoS ONE* **5**, e13761 (2010).
12. Wu, C., Ivanova, E., Cui, J., Lu, Q. & Pan, Z.H. Action potential generation at an axon initial segment-like process in the axonless retinal AII amacrine cell. *J. Neurosci.* **31**, 14654–14659 (2011).
13. Ihara, K. *et al.* Evolution of the archaeal rhodopsins: evolution rate changes by gene duplication and functional differentiation. *J. Mol. Biol.* **285**, 163–174 (1999).
14. Miesenböck, G., De Angelis, D.A. & Rothman, J.E. Visualizing secretion and synaptic transmission with pH-sensitive green fluorescent proteins. *Nature* **394**, 192–195 (1998).
15. Kleinlogel, S. *et al.* A gene-fusion strategy for stoichiometric and co-localized expression of light-gated membrane proteins. *Nat. Methods* **8**, 1083–1088 (2011).
16. Takamori, S. VGLUTs: 'exciting' times for glutamatergic research? *Neurosci. Res.* **55**, 343–351 (2006).
17. Regehr, W.G. Short-term presynaptic plasticity. *Cold Spring Harb. Perspect. Biol.* **4**, a005702 (2012).
18. Wang, L., Tu, P., Bonet, L., Aubrey, K.R. & Supplisson, S. Cytosolic transmitter concentration regulates vesicle cycling at hippocampal GABAergic terminals. *Neuron* **80**, 143–158 (2013).
19. Herman, M.A., Ackermann, F., Trimbuch, T. & Rosenmund, C. Vesicular glutamate transporter expression level affects synaptic vesicle release probability at hippocampal synapses in culture. *J. Neurosci.* **34**, 11781–11791 (2014).
20. Cousin, M.A. & Nicholls, D.G. Synaptic vesicle recycling in cultured cerebellar granule cells: role of vesicular acidification and refilling. *J. Neurochem.* **69**, 1927–1935 (1997).
21. Zhou, Q., Petersen, C.C. & Nicoll, R.A. Effects of reduced vesicular filling on synaptic transmission in rat hippocampal neurones. *J. Physiol. (Lond.)* **525**, 195–206 (2000).
22. Heine, M. *et al.* Surface mobility of postsynaptic AMPARs tunes synaptic transmission. *Science* **320**, 201–205 (2008).
23. Liu, G., Choi, S. & Tsien, R.W. Variability of neurotransmitter concentration and nonsaturation of postsynaptic AMPA receptors at synapses in hippocampal cultures and slices. *Neuron* **22**, 395–409 (1999).
24. Rosenmund, C. & Stevens, C.F. Definition of the readily releasable pool of vesicles at hippocampal synapses. *Neuron* **16**, 1197–1207 (1996).
25. Metzelaar, M.J. *et al.* CD63 antigen. A novel lysosomal membrane glycoprotein, cloned by a screening procedure for intracellular antigens in eukaryotic cells. *J. Biol. Chem.* **266**, 3239–3245 (1991).
26. Mattis, J. *et al.* Principles for applying optogenetic tools derived from direct comparative analysis of microbial opsins. *Nat. Methods* **9**, 159–172 (2012).
27. Hoffmann, A., Hildebrandt, V., Heberle, J. & Buldt, G. Photoactive mitochondria: *in vivo* transfer of a light-driven proton pump into the inner mitochondrial membrane of *Schizosaccharomyces pombe*. *Proc. Natl. Acad. Sci. USA* **91**, 9367–9371 (1994).
28. Maycox, P.R., Deckwerth, T. & Jahn, R. Bacteriorhodopsin drives the glutamate transporter of synaptic vesicles after co-reconstitution. *EMBO J.* **9**, 1465–1469 (1990).
29. Moechars, D. *et al.* Vesicular glutamate transporter VGLUT2 expression levels control quantal size and neuropathic pain. *J. Neurosci.* **26**, 12055–12066 (2006).
30. Pothos, E.N. *et al.* Synaptic vesicle transporter expression regulates vesicle phenotype and quantal size. *J. Neurosci.* **20**, 7297–7306 (2000).
31. Wojcik, S.M. *et al.* An essential role for vesicular glutamate transporter 1 (VGLUT1) in postnatal development and control of quantal size. *Proc. Natl. Acad. Sci. USA* **101**, 7158–7163 (2004).
32. Palmer, M.J., Hull, C., Vigh, J. & von Gersdorff, H. Synaptic cleft acidification and modulation of short-term depression by exocytosed protons in retinal bipolar cells. *J. Neurosci.* **23**, 11332–11341 (2003).
33. Williams, J. How does a vesicle know it is full? *Neuron* **18**, 683–686 (1997).
34. Siksou, L. *et al.* A role for vesicular glutamate transporter 1 in synaptic vesicle clustering and mobility. *Eur. J. Neurosci.* **37**, 1631–1642 (2013).
35. Budzinski, K.L. *et al.* Large structural change in isolated synaptic vesicles upon loading with neurotransmitter. *Biophys. J.* **97**, 2577–2584 (2009).

© 2015 Nature America, Inc. All rights reserved. npg

36. Daniels, R.W. *et al.* Increased expression of the *Drosophila* vesicular glutamate transporter leads to excess glutamate release and a compensatory decrease in quantal content. *J. Neurosci.* **24**, 10466–10474 (2004).
37. Nelson, H. & Nelson, N. Disruption of genes encoding subunits of yeast vacuolar H^+-ATPase causes conditional lethality. *Proc. Natl. Acad. Sci. USA* **87**, 3503–3507 (1990).
38. Davies, S.A. *et al.* Analysis and inactivation of *vha55*, the gene encoding the vacuolar ATPase B-subunit in *Drosophila melanogaster* reveals a larval lethal phenotype. *J. Biol. Chem.* **271**, 30677–30684 (1996).
39. Inoue, H., Noumi, T., Nagata, M., Murakami, H. & Kanazawa, H. Targeted disruption of the gene encoding the proteolipid subunit of mouse vacuolar H^+-ATPase leads to early embryonic lethality. *Biochim. Biophys. Acta* **1413**, 130–138 (1999).
40. Poëa-Guyon, S. *et al.* The V-ATPase membrane domain is a sensor of granular pH that controls the exocytotic machinery. *J. Cell Biol.* **203**, 283–298 (2013).
41. Di Giovanni, J. *et al.* V-ATPase membrane sector associates with synaptobrevin to modulate neurotransmitter release. *Neuron* **67**, 268–279 (2010).
42. Hiesinger, P.R. *et al.* The v-ATPase V0 subunit a1 is required for a late step in synaptic vesicle exocytosis in *Drosophila*. *Cell* **121**, 607–620 (2005).
43. Kawasaki-Nishi, S., Nishi, T. & Forgac, M. Arg-735 of the 100-kDa subunit a of the yeast V-ATPase is essential for proton translocation. *Proc. Natl. Acad. Sci. USA* **98**, 12397–12402 (2001).
44. Kato, H.E. *et al.* Crystal structure of the channelrhodopsin light-gated cation channel. *Nature* **482**, 369–374 (2012).
45. Müller, M., Bamann, C., Bamberg, E. & Kuhlbrandt, W. Projection structure of channelrhodopsin-2 at 6 A resolution by electron crystallography. *J. Mol. Biol.* **414**, 86–95 (2011).
46. Yoshimura, K. & Kouyama, T. Structural role of bacterioruberin in the trimeric structure of archaerhodopsin-2. *J. Mol. Biol.* **375**, 1267–1281 (2008).
47. Pungercar, J.R. *et al.* Autocatalytic processing of procathepsin B is triggered by proenzyme activity. *FEBS J.* **276**, 660–668 (2009).
48. Weisz, O.A. Organelle acidification and disease. *Traffic* **4**, 57–64 (2003).
49. Jiang, L.W., Maher, V.M., McCormick, J.J. & Schindler, M. Alkalinization of the lysosomes is correlated with ras transformation of murine and human fibroblasts. *J. Biol. Chem.* **265**, 4775–4777 (1990).
50. Dehay, B. *et al.* Loss of P-type ATPase ATP13A2/PARK9 function induces general lysosomal deficiency and leads to Parkinson disease neurodegeneration. *Proc. Natl. Acad. Sci. USA* **109**, 9611–9616 (2012).

© 2015 Nature America, Inc. All rights reserved.
npg

ONLINE METHODS

Cloning strategy and virus production. To generate the pHoenix construct, we inserted Archaerhodopsin-3 (Arch3) from *Halorubrum sodomense* into the synaptophysin molecule. Since it has been reported that a sypHy version lacking the fourth transmembrane domain and thus the C terminus of synaptophysin is incorrectly targeted in neurons[51], we maintained the N and C termini of synaptophysin as trafficking signals. First we inserted a single transmembrane domain of the rat gastric H^+/K^+ ATPase β-subunit[52], which has previously been successfully used for tandem optogenetic constructs[15], into the rat synaptophysin-pHluorin 2x (sypHy2) construct[53] using AgeI sites, thereby replacing the second super-ecliptic pHluorin molecule. Next, we amplified Arch3 cDNA (from Addgene clone 22222) by PCR. The fragment was inserted C-terminal to the super-ecliptic pHluorin using BamHI and SplI sites. Finally, the red fluorescent marker mKate2 (ref. 54) was inserted at the cytosolic C terminus of Arch3 via SplI and HindIII.

CD63 cDNA was generated by TA cloning from mouse whole brain mRNA and transferred into a mammalian expression vector with a CMV promoter. As the large second luminal loop contains three potential N-linked glycosylation motives[25], we introduced AfeI and SacI restriction sites into the first luminal loop as insertion site for the optogenetic cassette encoding pHluorin, Arch3, mKate2 and the rat gastric H^+/K^+ ATPase β-subunit. To create CD63-pHluorin, the CD63-pHoenix construct was AgeI-digested, thereby removing Arch3, mKate2 and the H^+/K^+ ATPase β-subunit, and religated. All constructs were verified by sequencing. Plasmids encoding pHoenix (GenBank accession code KT880224), lyso-pHoenix (GenBank accession code KT880225) and lyso-pHluorin (GenBank accession code KT880226) can be obtained via Addgene.

Viral particles were provided by the Viral Core Facility (VCF) of the Charité Berlin. Lentivirus was produced according to published protocols[55], with minor modifications as follows. The coding sequences of pHoenix, sypHy (Addgene clone 24478) or Arch3-EGFP were transferred into a modified FUGW lentiviral expression vector[55] with the neuron-specific human synapsin promoter. The expression vector (20 μg) was cotransfected into HEK 293T cells with 5 μg each of the helper plasmids pCMVdR8.9 and pVSV.G using X-tremeGENE 9 DNA transfection reagent (Roche). Lentiviral particles were harvested from cultures maintained in Neurobasal-A supplemented with 2% B27 and 0.2% penicillin/streptomycin (all cell culture media from Invitrogen) at 32 °C and 5% CO_2 for 72 h. Supernatants were filtered and subsequently concentrated 20-fold using Amicon Ultra-15 centrifugal 10-kDa filter units. Aliquots of the lentivirus were shock-frozen and stored at −80 °C. Adeno-associated virus (AAV) serotype 9 was produced in HEK 293 cells transfected with polyethylenimine and the following plasmids: pAD deltaF6, pAAV2/9 (both from Penn Vector Core, University of Pennsylvania) and an AAV expression vector encoding pHoenix under the human synapsin promoter. After 48 h, cells were resuspended, collected by centrifugation and lysed in 50 mM Tris-Cl, 150 mM NaCl. Viral particles were purified using an iodixanol gradient purification process according to published protocols[56] and stored at 4 °C.

Cell culture. Animals were handled in accordance with the regulations of local authorities and the animal welfare committee of the Charité – Universitätsmedizin Berlin, Germany.

Autaptic cultures of primary hippocampal neurons. Low-density cultures of hippocampal neurons on glia cell microislands[57] were prepared from newborn C57/BL6-N mice of either sex as previously described[58]. Briefly, astrocytes were prepared from cortices and expanded in T75 bottles in Dulbecco's modified Eagle's medium (DMEM) supplemented with 10% FCS and 0.2% penicillin/streptomycin (Invitrogen). To obtain microisland cultures, coverslips were coated with a thin film of agarose. After drying the agarose, a pattern of 300-μm-diameter spots of growth-permissive substrate consisting of 0.7 mg ml^{-1} collagen and 0.1 mg ml^{-1} poly-D-lysine was applied using a custom-made stamp. After 14 days *in vitro* (DIV), astrocytes were seeded onto the glass coverslips at a density of 5,000 cm^{-2} and were allowed to proliferate in DMEM medium for 1 week more to form microislands. Medium was changed to Neurobasal-A supplemented with 2% B27 and 0.2% penicillin/streptomycin 24 h before hippocampal neurons prepared from P0 mice were added at a density of 300 cm^{-2}. Neurons were infected with lentiviral particles at DIV 1–2.

Cultures of HEK 293 and HeLa cells. Cell lines were maintained in DMEM supplemented with 10% FCS and 0.2% penicillin/streptomycin. For live-cell imaging and immunocytochemistry experiments, cells were seeded at low density onto coverslips coated with 0.7 mg ml^{-1} collagen and 0.1 mg ml^{-1} poly-D-lysine, transfected after 24 h using X-tremeGENE 9 DNA transfection reagent according to the manufacturer's instructions, and used 24–48 h after transfection.

Hippocampal organotypic slice cultures. Wistar rat hippocampi were dissected from pups of either sex (postnatal day 5–8) in a sucrose-based solution and horizontal slices were cut using a vibratome (Leica VT1200S). Slices were washed with sterile solution and plated on membrane inserts (0.4 μm Millicell, Millipore). Culture medium contained 50% basal medium Eagle's (BME), 25% Hank's balanced salt solution (HBSS), 25% heat-inactivated horse serum, 1 mM Glutamax I supplement (all from GIBCO), and 6.5 g/L D-glucose. Antibiotics were added 24 h after the preparation (penicillin/streptomycin). The medium was changed three times a week. No antimycotics were used. At DIV 3–5 slices were transduced under sterile conditions with an AAV encoding pHoenix using a micromanipulator. The tip of a baked pipette was filled with the AAV-containing solution and lowered into stratum pyramidale of area CA3 so that the virus could diffuse into the slice.

Electrophysiology. Experiments on autaptic neurons were performed at room temperature on an Olympus IX51 inverted microscope equipped with a Multiclamp 700B amplifier under control of a Digidata 1440 AD board and pClamp10 software (Molecular Devices). External solutions were applied using a custom-built rapid perfusion system[58], while the bath level was controlled by an MPCU bath handler (Lorenz Messgerätebau, Katlenburg-Lindau, Germany). Whole-cell recordings were performed between DIV 14 and 21. Cells were voltage-clamped at −70 mV, with 70% compensation of series resistance and capacitance. Recordings were discarded when the series resistance exceeded 15 MΩ. To evoke EPSCs in autaptic neurons, unclamped action potentials were triggered by a 1-ms depolarization step to 0 mV. Spontaneous mEPSCs were analyzed from the same recordings in intervals starting 2 s after the action potential. Intracellular solution contained (in mM) 135 potassium gluconate, 17.8 HEPES, 1 EGTA, 4.6 $MgCl_2$, 4 Na_2-ATP, 12 creatine phosphate and 50 U/ml creatine phosphokinase, pH adjusted to 7.3 with KOH, 300 mOsm. Cells were continuously superfused with HEPES-buffered solution (in mM): 140 NaCl, 2.4 KCl, 10 HEPES, 10 glucose, 2 $CaCl_2$ and 4 $MgCl_2$, pH adjusted to 7.3 with NaOH, 300 mOsm. The readily releasable pool was determined as the charge transient of the postsynaptic current evoked by a 5-s application of 500 mM sucrose dissolved in extracellular solution, and the p_{vr} was calculated as the ratio of the EPSC charge and the sucrose-evoked charge[24]. The antagonist for AMPAR desensitization, cyclothiazide (Tocris), was used at 100 μM, and the low-affinity AMPAR antagonist γ-D-glutamylglycine (γ-DGG) at 500 μM. Data were sampled at 10 kHz and filtered at 3 kHz. Cultures were treated for 2–5 h with 1 μM bafilomycin A1 (Tocris, Bristol, UK; or Enzo Life Sciences, Farmingdale, NY, USA) before the recordings.

Hippocampal organotypic slice cultures were transferred to a submerged recording chamber on an upright Olympus BX51 microscope and continuously perfused with ACSF: in mM, 125 NaCl, 25 $NaHCO_3$, 3 KCl, 1.25 NaH_2PO_4, 2 $CaCl_2$, 1 $MgCl_2$ and 10 glucose, oxygenated at 95% O_2 and 5% CO_2. Whole-cell recordings from CA3 neurons were performed at room temperature with an Axon Multiclamp 700B amplifier. Intracellular solution contained (in mM) 135 potassium gluconate, 7 NaCl, 10 HEPES, 2 Na_2-ATP, 0.3 Na-GTP and 2 $MgCl_2$, pH adjusted to 7.2–7.3 with KOH. The stimulation electrode was placed in stratum radiatum and action potentials were triggered at 0.1 Hz. Stimulus intensities were adjusted to values similar to those used in control slices without treatment of Baf.

Light delivery and live cell imaging. In electrophysiological experiments on autaptic neurons without imaging, we activated pHoenix using a mercury lamp for illumination controlled by a TTL-controlled mechanical shutter (Uniblitz, Vincent Associates, NY, USA). Excitation light was passed through a 25% neutral density filter (Olympus) and a 546/10 nm excitation filter (11002v2-Green, Chroma Technology, Bellows Falls, VT, USA). The light intensity above the objective (Olympus UPLSAPO 20×, 0.75 NA) was 265 mW cm^{-2} at 546 nm. Similarly, organotypic hippocampal slices were illuminated through the objective (Olympus LumPlan FI 60X, 0.9 NA water immersion) with a mercury lamp controlled by a TTL-driven mechanical shutter, using a 587/25 nm excitation filter (F20-451, AHF Analysentechnik, Tübingen, Germany).

For electrophysiology experiments and parallel imaging of pHluorin signals in autaptic neurons, we used an Olympus UPLSAPO 60×, 1.2 NA water immersion

© 2015 Nature America, Inc. All rights reserved.

npg

objective. A TTL-controlled LED system (pE2, CoolLED, Andover, UK) equipped with a 490-nm LED and a broadband GYR LED was coupled into the back port of the microscope. Excitation and emission light was separated by a multiband dichroic mirror (F72-628, AHF Analysentechnik, Tübingen, Germany). We found that band-pass filters (blue LED: excitation filter of the AHF Tripleband Filterset F69-402 with 495/10; GYR-LED: AHF F47-605 with 605/70) prevented unintended Arch3 activation by the blue LED, allowed optimal Arch3 activation and minimized bleaching of pHluorin molecules by the yellow LED. Fluorescence signals of pHluorin molecules were band-pass filtered (AHF F73-402) and imaged with an EMCCD camera (iXon 897, Andor, Belfast, UK) using Micromanager software[59]. During reacidification experiments, pHluorin signals were captured at 0.2 Hz, except for experiments in **Supplementary Figure 4** (0.05 Hz). After acquisition of baseline pHluorin signals, pHoenix was activated by a near-continuous illumination with the GYR-LED, which was briefly interrupted at 0.2 or 0.05 Hz by 100 ms flashes of the 490 nm LED. The following LED settings were applied for these imaging experiments: 490 nm LED set to 10–20% (50–100 mW cm^{-2}); GYR-LED set to 100% (1,100 mW cm^{-2} at 580 nm), 4.8 or 19.8 s exposure at 0.2 or 0.05 Hz respectively. GYR-LED was set to 10% for low light intensity experiments presented in **Supplementary Figure 7**. Intensities were measured above the objective. For the EMCCD, we used the following settings: 100 ms exposure synchronized with the 490 nm LED, 2 × 2 bin, −80 °C, 4.7× pregain; EMgain 300 for pHoenix imaging, 100 for sypHy imaging. The same imaging setup was used for experiments on HEK 293 cells expressing lyso-pHoenix.

We determined the fraction of surface-resident pHoenix or sypHy molecules by applying an extracellular solution buffered with 10 mM MES instead of HEPES at pH 5.5, followed by the application of 50 mM NH_4Cl containing extracellular solution with NaCl reduced to 90 mM to maintain the osmolarity[60]. Images were acquired at 2 Hz during the pH 5.5 NH_4 protocol.

Immunocytochemistry. High-density cultures of pHoenix- and Arch3-expressing hippocampal neurons were fixed at DIV 14 with 3% (w/v) paraformaldehyde for 10–15 min at room temperature. Fixed samples were stained with primary antibodies against VGLUT1 (no. 135 302, Synaptic Systems, Göttingen, Germany) and MAP2 (AB5543, Chemicon by Merck Millipore, Darmstadt, Germany) and secondary antibodies coupled to Alexa Fluor 647 or Dylight-405 (no. 711-605-152 and no. 711-475-152, respectively, Jackson ImmunoResearch, West Grove, PA, USA). Stained samples were mounted in Mowiol. Fluorescent specimens were examined under a confocal laser-scanning microscope (TCS SP5, Leica, Wetzlar, Germany). 1024 × 1024 pixel images were acquired using a 63×, 1.4 NA oil immersion objective and a 2–4× zoom.

Lyso-pHoenix transfected HeLa cells were fixed 24 h after transfection with 4% (w/v) paraformaldehyde for 12 min at room temperature or with methanol for 15 min at −20 °C. The following primary antibodies were used: antibodies against GFP (no. A-11122, Life Technologies), human CD107b (lysosome-associated membrane protein-2, LAMP-2; no. 10-672-C100, HISS Diagnostics), human Rab-5 (no. 108011, Synaptic Systems), human PDI (no. MA 3-019, Affinity BioReagents), human GM-130 (no. 610823, BD Biosciences) and human Hsp-60 (no. 611563, BD Biosciences). Secondary antibodies were coupled to Alexa 488 (no. A11034) and Alexa 633 (no. A21052, both Life Technologies, Molecular Probes, Carlsbad, CA, USA) respectively. For imaging, the cells were mounted with Aqua Poly Mount (no. 633736, Polysciences, Warrington, PA, USA). Images were acquired with a laser-scanning confocal microscope (LSM510, Carl Zeiss, Jena, Germany) equipped with a 63×, 1.4 NA oil immersion objective. The image size was set to 1024 × 1024 pixels. Images for figures were processed with ImageJ software (ImageJ 1.47t; NIH, USA) to enhance brightness using the brightness/contrast function. Immunocytochemistry experiments were repeated two to three times.

Data collection and analysis. Viral particles encoding controls and pHoenix constructs were randomly applied on different wells of the same 6- or 12 well plates from the same culture. From each culture, wells were randomly subjected to treatment or control conditions, and recordings from multiple groups were performed on the same day in a randomized order. Data collection and analysis were not performed blind to the conditions of the experiments.

Electrophysiological recordings were analyzed using the AxographX software. For mEPSC analysis, we used the implemented scaled template detection algorithm for recordings that had been filtered once *post hoc* with a 1-kHz low-pass filter. False-positive events were estimated by running the spontaneous event detection with an inverted template[61]. Frequency and amplitude of mEPSCs were corrected for false positives, and recordings with false-positive events of >2 Hz were excluded.

Images of pHluorin signals were analyzed using ImageJ and the Time Series Analyzer V2.0 plug-in. Fluorescence intensities were calculated from 2 × 2 pixel regions of interest (ROI) drawn on synaptic contacts, which were identified as small structures with a dynamic increase of fluorescence evoked by NH_4Cl application. Background fluorescence from a region with no neuronal structures was subtracted for each frame.

Colocalization of lyso-pHoenix and organelle markers was analyzed using the CellProfiler 2.1.1 program (Broad Institute of MIT and Harvard)[62]. In a pixel-based approach, the colocalization of two channels was calculated after the images were aligned. For every co-staining, ten cells were analyzed and the Pearson's correlation coefficient was determined.

Data are presented as mean ± s.e.m. and were tested for normality using the D'Agostino and Pearson omnibus normality test. Sample sizes were not predetermined by statistical methods but are similar to those reported in comparable previous publications[15]. Time constants were calculated by fitting the data as a monoexponential decay or association using GraphPad Prism 5. Differences between two groups were tested for significance by unpaired or paired two-way Student's *t*-tests. If data did not pass the normality test, we applied a Mann-Whitney *U* test for unpaired data and a Wilcoxon signed-rank test for paired. For multiple comparisons of EPSC amplitudes and mEPSC frequencies in **Supplementary Figure 5**, we used repeated-measures two-way ANOVA with Sidak's multiple comparisons post-test, and a regular two-way ANOVA with Sidak's multiple comparisons post-test for comparisons of mEPSC amplitudes (because there were three Baf-treated cells without detectable mEPSCs in the pre-light condition, repeated measures two-way ANOVA could not be performed for mEPSC amplitudes). Number of cells (*n*) and number of cultures (*N*) are reported in the figure legends. Statistics were calculated using GraphPad Prism 5 and 6.

A **Supplementary Methods Checklist** is available.

51. Royle, S.J., Granseth, B., Odermatt, B., Derevier, A. & Lagnado, L. Imaging pHluorin-based probes at hippocampal synapses. *Methods Mol. Biol.* **457**, 293–303 (2008).
52. Shull, G.E. cDNA cloning of the beta-subunit of the rat gastric H,K-ATPase. *J. Biol. Chem.* **265**, 12123–12126 (1990).
53. Zhu, Y., Xu, J. & Heinemann, S.F. Two pathways of synaptic vesicle retrieval revealed by single-vesicle imaging. *Neuron* **61**, 397–411 (2009).
54. Shcherbo, D. *et al.* Far-red fluorescent tags for protein imaging in living tissues. *Biochem. J.* **418**, 567–574 (2009).
55. Lois, C., Hong, E.J., Pease, S., Brown, E.J. & Baltimore, D. Germline transmission and tissue-specific expression of transgenes delivered by lentiviral vectors. *Science* **295**, 868–872 (2002).
56. Lock, M. *et al.* Rapid, simple, and versatile manufacturing of recombinant adeno-associated viral vectors at scale. *Hum. Gene Ther.* **21**, 1259–1271 (2010).
57. Bekkers, J.M. & Stevens, C.F. Excitatory and inhibitory autaptic currents in isolated hippocampal neurons maintained in cell culture. *Proc. Natl. Acad. Sci. USA* **88**, 7834–7838 (1991).
58. Rost, B.R. *et al.* Autaptic cultures of single hippocampal granule cells of mice and rats. *Eur. J. Neurosci.* **32**, 939–947 (2010).
59. Edelstein, A., Amodaj, N., Hoover, K., Vale, R. & Stuurman, N. Computer control of microscopes using microManager. *Curr. Protoc. Mol. Biol.* Ch. 14, Unit 14.20 (2010).
60. Sankaranarayanan, S., De Angelis, D., Rothman, J.E. & Ryan, T.A. The use of pHluorins for optical measurements of presynaptic activity. *Biophys. J.* **79**, 2199–2208 (2000).
61. Clements, J.D. & Bekkers, J.M. Detection of spontaneous synaptic events with an optimally scaled template. *Biophys. J.* **73**, 220–229 (1997).
62. Carpenter, A.E. *et al.* CellProfiler: image analysis software for identifying and quantifying cell phenotypes. *Genome Biol.* **7**, R100 (2006).

© 2015 Nature America, Inc. All rights reserved.

npg

doi:10.1038/nn.4161